SPATIAL-SPECTRAL HYPERSPECTRAL IMAGE CLUSTERING USING CLUSTER'S BANDS BOX-PLOTS

Mohamed A. Al Moghalis[1], Osman M. Hegazy[2], Ibrahim F. Imam[3] and Ali H. el-Bastawessy[3]
[1]*Lecturer of Information Systems, Dep.of Information Systems,*
College of Computer and Information Systems, Alyamamah University, KSA.
[2]*Professor of Information Systems, Dep. of Information Systems,*
Faculty of Computers and Information, Cairo University, Egypt.
[3]*Professor of Computer Science, Dep. of Computer Science, College of Computing and Information Technology,*
Arab Academy for Science, Technology and Maritime Transport, Egypt.
[4]*Professor of Information Systems, Dean of the Faculty of Computer Science MSA University, Egypt.*

ABSTRACT

The attention given recently for Hyperspectral Images (HSI) in remote sensing was due to its spectral nature used in earth surface exploration. Recently, researches proposed approaches that combine features of spatial nature with spectral nature to enhance HSI analysis accuracy. The reason behind this orientation is that contiguous pixels mostly share spectral features due to the low spatial resolution.
In this paper, authors follow this orientation in clustering HSI using K-means. The proposed approach uses kernels, group of spatially neighbored pixels, to build profile for each cluster. The profile preserves cluster's spectral nature through its bands' Box-Plots that were extracted from selected kernels. The approach starts by selecting K kernels from the given image scene randomly instead of generating random kernels. Then a profile for each cluster is built using the selected kernel pixels' spectrums. The profile consists of *b* box-plots, where *b* is the number of bands. Each band box-plot interprets the spread of contiguous pixels' reflectance values in that band. Each pixel in the image will join the nearest cluster. The distance to be measured between any given pixel spectrum and cluster's centroid is replaced by counting how many reflectance values have been considered outlier to their corresponding band's box-plot in that cluster profile. The pixel will join the cluster with minimum outlier count. The profiles are updated iteratively using the new pixels distribution. Data sets used in the experiments are captured by Hyperion Earth Observer 1 (EO-1) sensor.

KEYWORDS

Hyperspectral Images, clustering, image processing, k-means, remote sensing

1. INTRODUCTION

Hyperspectral images (HSI) used in this paper are image scenes obtained remotely for Earth across many electromagnetic bands. The advance in these images is that they capture the reflectance values for light energy over wide spectrum range beyond human vision ability. The spectrum is divided into contiguous wavelength intervals named bands. The number of bands is the spectral resolution. The point of interest is that each material on Earth has a unique spectral signature. The signature is obtained by plotting reflectance values against wavelength. In other words, HSI consists of thousands or even millions of pixels. Each pixel in turn contains hundreds of reflected electromagnetic energy at hundreds narrow contiguous bands. Each value is the energy reflected at a certain wavelength interval. HSI can be seen as an image cube or layers of the same image as exhibited in figure 1. Each layer represents the image in a certain band. The spatial resolution of HSI is the geographical area covered by a single pixel on the Earth. The spectral dimension can be considered as the third dimension in the image cube.

ISBN: 978-989-8704-10-8 © 2014

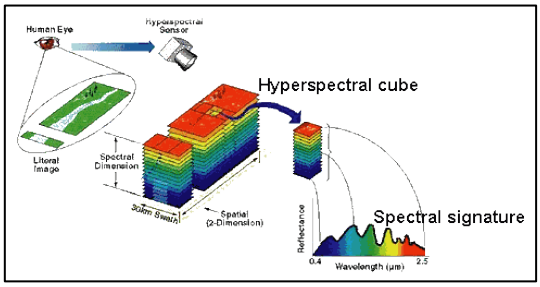

Figure 1. Hyperspectral image structure.

Research associations started building libraries of pure materials signatures to be used in HSI analysis. Due to low spatial resolution, HSI pixel spectrum may contain a mixture of different materials signatures. The mixed problem is investigated in the field of Spectral Unmixing. Other trends are classification, target detection, clustering, segmentation, data compression and dimensionality reduction. The technology of both parallel and distributed processing is utilized to acquire faster analysis results. Hyperspectral remote sensing technology is applied in a wide range of application including agriculture, medicine, food quality control, remote mineral exploration and environmental monitoring applications.

2. RELATED WORK

In the last decade, research in HSI tended towards squeezing Hyperspectral data for more information. This is because of both limitation of spatial resolution and Earth heterogeneity. Exploiting both spatial and spectral contexts together was encouraged by the accuracy improvement. The availability of parallel computation power has facilitated the application of algorithms known by complex computation. Spatial context has been used recently to enhance results extracted from spectral context. The framework proposed by Plaza et al used both spectral and spatial data for classification using Active Learning algorithms (AL) to exploit both contexts through marginal probability distribution [1]. Pixel kernel neighborhood was used by Fauvela et al. to join both spectral and spatial information in Support Vector Machine (SVM) classification showing improvements in accuracy [2].

In spectral unmixing, authors of [3] used spatial context to identify local endmembers instead of global ones. The relationship between pixels in same neighborhood was exploited to enhance classification using Iterative Conditional Modes [4]. Results were sensitive to the level of both homogeneity and spatial correlation. Spatial correlation between pixels was exploited using a Bayesian model introduced in [5]. Spatial dependency of class's pixels was modeled using Markov random field. The framework for spectral-spatial classification by authors in [6] used extracted spatial information through morphological APs. In another framework for classification with SVM that consider both global and local posterior probabilities distribution, the impact of local irrelevant classes are removed while enhancing local relevant classes impact [7]. Probabilistic classification on pixel wise is performed first followed by hierarchical step-wise optimization algorithm that merges the spatially neighboring regions iteratively [8]. Pixel wise classification accuracy was increased by providing more homogeneous regions classification maps [9]. Results were better for images with large spatial structures and when classes differently responses spectrally through pixels. Many researches still emphasize on spatial context added value to the exploitation of Hyperspectral images [10, 11].

3. HSI CLUSTERING USING BOX-PLOT

3.1 Box-Plot Analysis

The spread of data elements in space can be interpreted using different techniques. In Box-Plot analysis, data elements are ordered either ascending or descending. Upper Quartile (UQ) and Lower Quartile (LQ)

represent the 75th and 25th elements respectively. Inter Quartile Range (IQR) is the difference between UQ and LQ. LQ and UQ are used to define Lower Outer Fence (LOF), Lower Inner Fence (LIF), Upper Outer Fence (UOF) and Upper Inner Fence (UIF) using the following equations:

- Lower Inner Fence (LIF) = LQ - 1.5 × IQR
- Upper Inner Fence (UIF) = UQ + 1.5 × IQR
- Lower Outer Fence (LOF) = LQ – 3 × IQR
- Upper Outer Fence (UOF) = UQ + 3 × IQR

Box-plot fences define outliers. Data element lies beyond inner fences is called *mild outlier* and is called *extreme outlier* if it lies beyond outer fences as shown in figure 2.

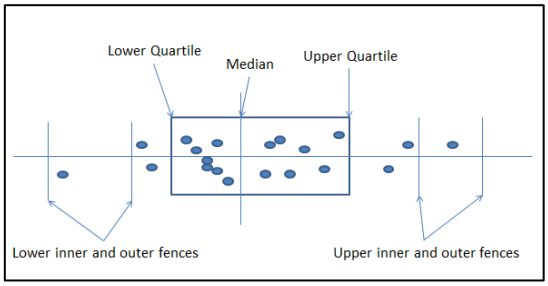

Figure 2. Box-Plot Analysis.

3.2 Kernel Analysis

Given HSI scene, a kernel is selected randomly from the scene. Each kernel is a group of neighbor pixels surrounding a center pixel with indices *(i, j)*, where *i* is the row index and *j* is the column index. The kernel used in this paper is of 8 pixels pattern. The neighborhood for a single band is shown in figure 3a. For *b* bands, the kernel consists of a set of *b* layers as shown in Figure 3b. Figure 3c shows a kernel chosen randomly from data set 1. It shows similar pixels spectrums. In fact this similarity depends on the spatial resolution and on the homogeneity of image kernel pixels. For each band in the kernel, box-plot analysis is applied to interpret reflectance value distribution in this band. Next section will explain in details how this is applied in the experiment.

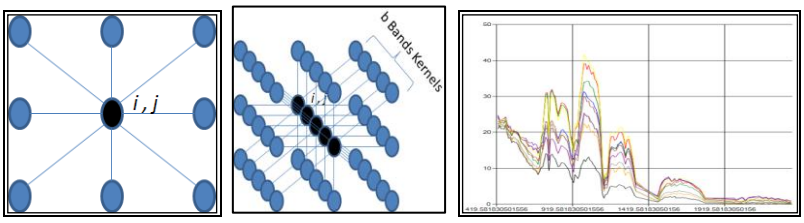

Figure 3. a) 8-pattern Kernel for single band.b) 8-pattern Kernel of b bands.c) Random kernel pixels Plot from data set 1.

3.3 Kernel Box-Plot Clustering

In this paper, kernels selected randomly from the given scene are used as initial centroids instead of generating random cluster kernels profiles. K kernels are selected from the image scene; each kernel will represent a cluster. A profile consists of b box-plots is built using kernel's pixels' reflectance values. For each band in a given kernel or cluster, a box-plot is built using the neighborhood pixels' values in this band. After all profiles have been built for all clusters, the approach starts clustering image pixels iteratively as follows. The distance measure, that will specify the cluster to which a pixel belongs, is the number of this pixel's values that were declared as outliers to correspondent band box-plot profile. The steps of the proposed approach are described in figure 4a. The scheme of clustering a pixel is shown in figure 4b.

For a given pixel (*i, j*) with *B* bands, each value in band b_n, n=1, 2, 3….,*B*, will be mapped to its corresponding band box-plot of the first cluster followed by other clusters. For each cluster, a counter NOB (Number of Outlier Bands) will register how many box-plots detected a pixel's value as mild outlier or

extreme outlier. In other words, NOB is the number of outlier pixel's values in a given cluster. The pixel (*i, j)* will join the cluster with the minimum NOB or the nearest cluster if we can say so. After all pixels have been divided between clusters, the clusters' profiles will be updated using newly joined pixels. Then the first iteration is complete. The process will iterate till no change or a threshold reached as shown in Figure 4a. The next section will discuss data sets and results obtained both qualitatively and quantitatively.

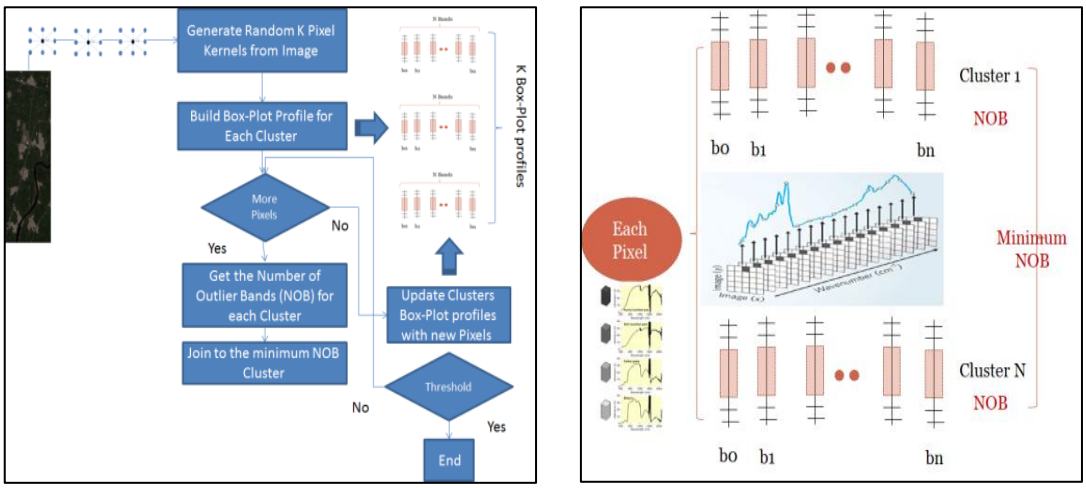

Figure 4. a) Box-plot clustering flow chart. b) Pixel comparison scheme against clusters' profiles.

4. EXPERIMENT AND RESULTS

The described approach in the previous section was applied on two data sets captured by EO-1 sensor. They will be referred to as data set 1 and data set 2 respectively. The first data set is a region subset in Delta area in Egypt and is shown in figure 6a. The second data set is a region subset from France and is shown in figure 7a. Both data sets were selected randomly. The results are compared to the output of ENVI commercial software using confusion matrix. This is because we didn't have real ground truth data. ENVI clustering output was generated using k-means. In this section we will start with the qualitative evaluation followed by the quantitative evaluation using confusion matrix. The colors of both ENVI and the proposed approach outputs are not matched. A cluster with green color in one picture might occur with red color in another picture. So we depend on visual detection of clusters. The visual detection mapping is used in confusion matrix to compare results of the proposed approach with ENVI output. This section will include both qualitative and quantitative evaluation followed by conclusion.

4.1 Earth Observer -1 Sensor (EO-1)

HSI data sets used in the experiments are captured by Hyperion Earth Observer 1 (EO-1) sensor. EO-1 has a spatial resolution of 30m×30m per pixel. Practically, this area may contain a mixture of different materials like buildings, roads, rivers ...etc. EO-1 spectral resolution is 242 bands. Each band is a 10 nm interval on light spectrum. Data set 1 consists of 158 bands each of 358 lines and 167. This is 59,786 pixels. Data set 2 consists of 155 bands each of 241 lines and 392. This is 94,472 pixels.

4.2 Results

4.2.1 ENVI Clustering

In figure 5, six clustering output from ENVI are demonstrated for data set 1. The first three, from left to right, are the results of ENVI k-means algorithm with three, four and five clusters respectively. The other three images to the right are results of ENVI ISO algorithm with same cluster numbers. The number of iterations in

both algorithms used is ten. Both clustering algorithms showed river, road and some urban areas belong to the same cluster in red.

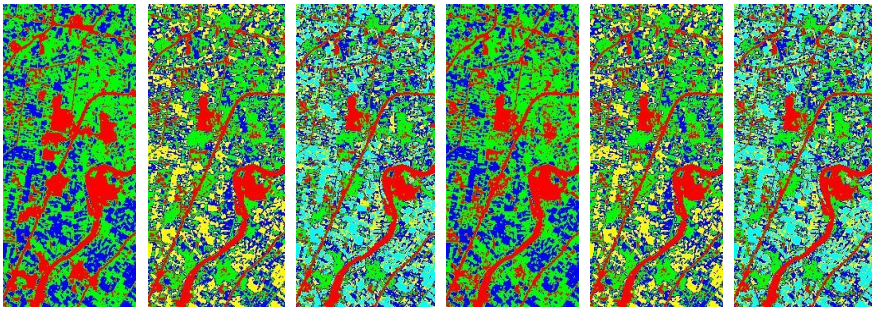

Figure 5. ENVI Unsupervised K-means and ISO output for data set 1.

4.2.2 Box-Plot Clustering

The proposed approach is applied on both data sets. Kernel sizes used for qualitative evaluation are 3 × 3, 5×5 and 7 × 7. The number of clusters requested was 7. K-means algorithm was applied as well using ENVI with the same cluster number and iterations. Image results for data set 1 are shown in figure 6. Figure 6b shows the results of 7 clusters and kernel size 3 × 3. Kernel size was increased to 5 × 5 and 7 × 7 in Figures 6c and 6d respectively with the same clusters number. K-means algorithm was applied by ENVI with same number of clusters. The result is shown in figure 6e. Figures 6b, 6c and 6d used different random kernels and 10 iterations.

Using ENVI output as a benchmark along with original image; Primary results showed in figure 6 are considered encouraging as the details from original image are preserved can be detected by human eye. As the number of clusters increase, more details are obtained. In ENVI output, figure 6e, the street and river joined the same cluster. The cluster is colored in red. Of course, we aren't judging ENVI or explaining its results. However, the proposed approach overcomes ENVI in differentiating between them as shown in figures 6b, 6c and 6d. The river appears in the original image in black color that starts from the middle of right side of figure 6a to the first quarter of the figure bottom. River is shown in blue, green and black in figures 6b, 6c and 6d respectively. Applying same experiment to data set 2; primary results are shown in figure 7. The difference here is that figure 7b, 7c and 7d are initial results without iterations. Results in figure 7b, 7c and 7d look the same as ENVI output in figure 7e. Water repositories were defined similar to ENVI output. On the other hand, there are still some differences in other areas.

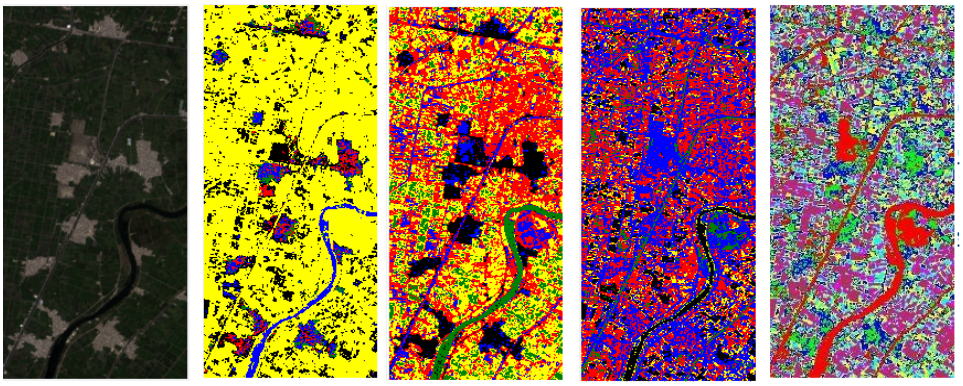

Figure 6. a) Data set 1 original Image. b) Data set 1 output for 7 clusters using 3 × 3 kernel size. c) Data set 1 output for 7 clusters using 5 × 5 kernel size. d) Data set 1 output for 7 clusters using 7 × 7 kernel. e) Data set 1 output for 7 clusters using ENVI k-means.

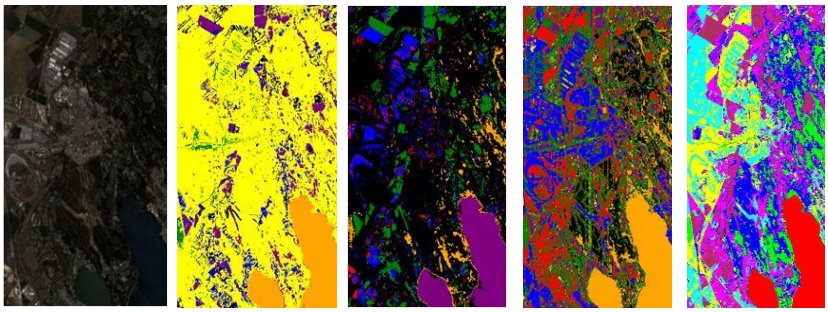

Figure 7. a) Data set 1 original Image. b) Data set 1 output for 7 clusters using 3 × 3 kernel size. c) Data set 1 output for 7 clusters using 5 × 5 kernel size. d) Data set 1 output for 7 clusters using 7 × 7 kernel. e) Data set 1 output for 7 clusters using ENVI k-means.

During experiments, some factors were identified that affect accuracy. The proposed approach is strongly affected by initial selection of kernels and their pixels. Selected kernel might be representing a cluster that is already represented by another kernel. This will lead some clusters to merge through iterations. Moreover, unrepresented cluster's pixels will join the wrong cluster. Another factor that affects the approach is the degree of how selected kernel's pixels are similar to each other. In other words, the kernel may include pixels of different clusters. In that case, the profile that will be built using these pixel's spectrums will represent more than one cluster and box-plots will contain wider range. In some cases, this profile absorbed pixels from their correct clusters to join it. The effect of these factors is shown in figures 8 and 9. In figure 8, the approach was applied to data set 1. 5 kernels were initially selected. The output was only four clusters in colors red, green, blue and black. The fifth cluster included zero pixels. One cluster represented river, urban areas and roads and is shown in red color. Figure 9 shows another run on the same data set. The negative effect is shown at the fifth iteration output is shown in figure 9f. The experiment ended with only three clusters. A third run, on the same data set, with the same number of clusters and appropriate initial kernels, generated better results. The result is shown in Figure 9. However, an appropriate selection of initial kernels would end with better clustering results as shown in figure 10. Reader would notice that some agriculture fields join the same cluster with river in blue color. This is because some agricultures fields in Egypt need to be withdrawn with water. Another notice that river contains small islands that contain small farms and few buildings. Output in figure 10 is considered of high quality. The next section will contain qualitative analysis of the proposed approach.

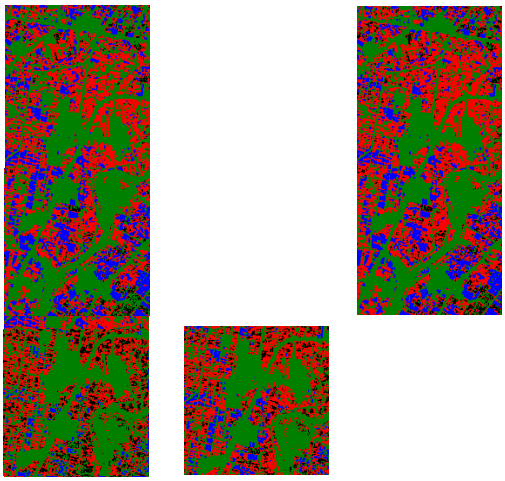

Figure 8. a) Initial run on data set 1. b) First iteration output. c) Second iteration output. d) Third iteration output. e) Fourth iteration output. f) Fifth iteration output.

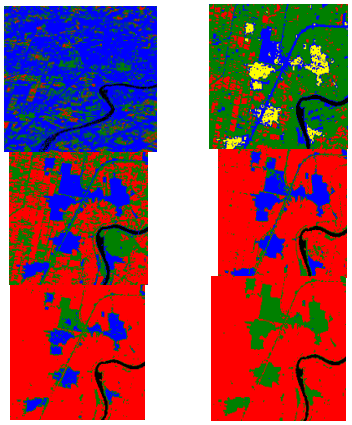

Figure 9. a) Another run on data set 1. b) First iteration output. c) Second iteration output. d) Third iteration output. e) Fourth iteration output. f) Fifth iteration output.

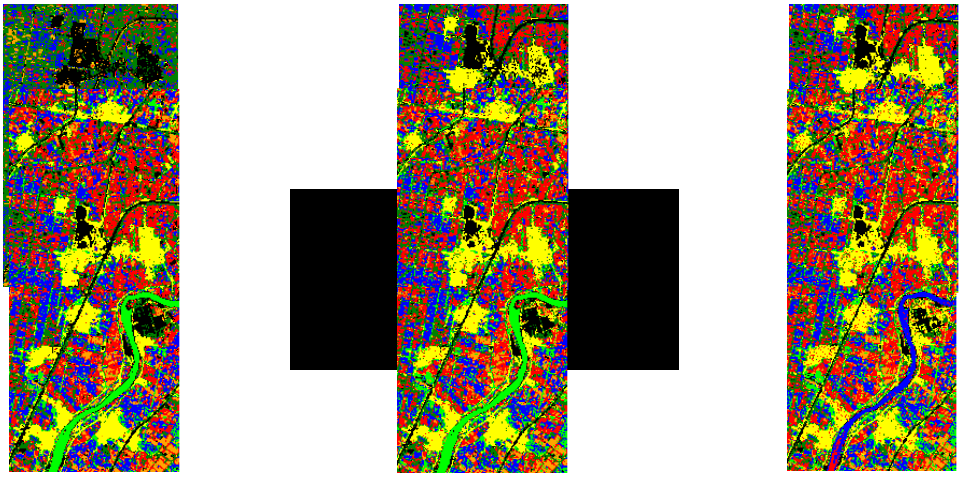

Figure 10. a) Initial run for appropriate selected kernels on data set 1. b) First iteration output. c) Second iteration output. d) Third iteration output. e) Fourth iteration output. f) Fifth iteration output.

4.2.3 Quantitative Analysis

In order to obtain a quantitative evaluation, experiments need ground truth information. Unfortunately, this was not available till the time of writing this paper. Instead, results are compared to ENVI output for the same data sets. User interaction was required to obtain better results. Initial kernels selection was guided by ENVI output. Data set 1 was divided into three clusters using both ENVI and the proposed approach. Results are shown in figures 11a and 11b respectively. It is noted in ENVI output that the river was grouped in the same cluster of buildings and highway with red color. On the other hand, it was grouped in the same cluster of some agriculture fields using the proposed approach. The last case is more reasonable as some agriculture fields are drawn with water depending on crop's type. This would be a strength point for the proposed approach. However, ENVI was considered as ground truth information. The overall accuracy using confusion matrix was 73.191%. Confusion matrix analyzes the distribution of pixels between the two outputs after mapping the classes, as colors are different. Details are shown in table 1. If box-plot clustering output was considered as the ground truth information, ENVI's total accuracy was 76.83%. Following the same comparison with data set 2; box-plot clustering output achieved 55.57% accuracy. Again, if box-plot clustering output is considered as the ground truth information, ENVI's total accuracy was 55.57%. Table 2 exhibits the confusion matrix for data set 2.

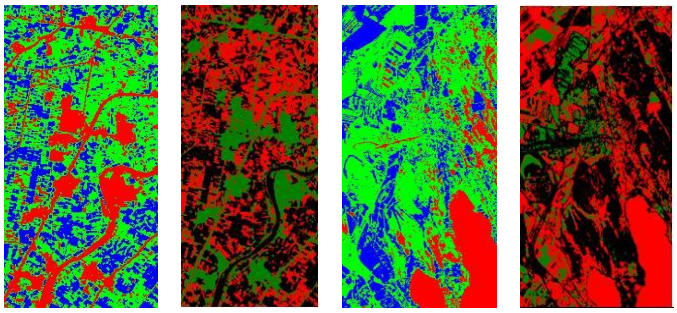

Figure 11. a) ENVI output for data set 1 with three clusters. b) Proposed approach output for data set 1 with three clusters. c) ENVI output for data set 2 with three clusters. d) Proposed approach output for data set 2 with three clusters.

Table 1. Data set 1 confusion matrix

	Ground Truth (Pixels)				
Class	Unclassified	Class 1	Class 2	Class 3	Total
Unclassified	0	0	0	0	0
Class 1	0	9992	5316	0	15308
Class 2	0	2998	17573	88	20659
Class 3	0	1519	6107	16193	23819
Total	0	14509	28996	16281	59786

Table 2. Data set 2 confusion matrix

	Ground Truth (Pixels)				
Class	Unclassified	Class 1	Class 2	Class 3	Total
Unclassified	0	0	0	0	0
Class 1	0	9134	10080	18429	37643
Class 2	0	8525	36815	7	45347
Class 3	0	115	4814	6553	11482
Total	0	17774	51709	24989	94472

5. CONCLUSION

Experiments' results have shown that the proposed approach is affected by initial random selection of kernels. The selection could cause repeated class representation neglecting other classes. As a result, pixels that belong to a neglected class joined the incorrect class instead. Moreover, represented class profiles with false pixels will be more generic. In such case, iterations will yield smooth homogeneous areas. Another factor affecting the proposed approach is the degree of similarity between pixels of a selected kernel. Cluster profile created using this kernel will represent more than one cluster and may absorb pixels from their real cluster. In addition, the sufficient number of kernels needed to represent all classes is still unknown.

However, quantitative evaluation results have encouraged proposing the approach of this paper. Using appropriate number of clusters and well selected kernels to represent them, results' quality is competing with ENVI output. Although ENVI clustering output for data set 1 was not reasonable for some classes, it was considered as a ground truth in the experiments due to the lack of real ground truth data. The proposed approach scored accuracy of 73.191% in data set 1 and 55.57% in data set 2. The approach still needs enhancements to overcome some weaknesses points but results can be considered encouraging.

REFERENCES

[1] J. Li, M. Bioucas-Dias, and A. Plaza, 2013. Spectral–Spatial Classification of Hyperspectral Data Using Loopy Belief Propagation and Active Learning. In *IEEE Transactions on Geoscience and Remote Sensing*, Vol. 51, No. 2, pp 844-856.

[2] M. Fauvela, J. Chanussotb and J.A. Benediktssonc, 2012. A Spatial-Spectral Kernel Based Approach for the Classification of Remote Sensing Images. In *Journal of Pattern Recognition*, Vol. 45, pp 381-392.

[3] K. Canham, A. Schlamm, B. Basener and D. Messinger, 2011. High spatial resolution hyperspectral spatially adaptive endmember selection and spectral unmixing. Proceedings of *SPIE 8048, Algorithms and Technologies for Multispectral, Hyperspectral, and Ultraspectral Imagery* XVII, 80481O.

[4] S. Magnussen, P. Boudewyn and M. Wulder, 2004. Contextual classification of Landsat TM images to forest inventory cover types. In *International Journal of Remote Sensing*, Vol. 25, Issue 12, pp. 2421-2440.

[5] O. Eches, N. Dobigeon and J. Tourneret, 2011. Enhancing hyperspectral image unmixing with spatial correlations. In *IEEE Transactions on Geoscience & Remote Sensing*, Vol. 49, pp. 4239-4247.

[6] P. Ghamisi, J. Benediktsson, G. Cavallaro and A. Plaza, 2014. Automatic Framework for Spectral–Spatial Classification Based on Supervised Feature Extraction and Morphological Attribute Profiles. In *IEEE Journal of Selected Topics in Applied Earth Observations and Remote Sensing*.

[7] M. Khodadadzadeh, J. Li, A. Plaza, H. Ghassemian, M. Bioucas-Dias and X. Li, 2014. Spectral–Spatial Classification of Hyperspectral Data Using Local and Global Probabilities for Mixed Pixel Characterization. In *IEEE Transactions on Geoscience and Remote Sensing*.

[8] Y. Tarabalka and C. Tilton, 2011. Spectral-Spatial Classification of Hyperspectral Images Using Hierarchical Optimization. Proceedings of *Hyperspectral Image and Signal Processing: Evolution in Remote Sensing*, Lisbon, Portugal.

[9] Y. Tarabalka, J. Benediktsson, and J. Chanussot, 2009. Spectral spatial classification of hyperspectral imagery based on partitional clustering techniques. In *IEEE Trans. Geos. and Remote Sensing*, Vol. 47, pp 2973–2987.

[10] Baowei Fei, Akbari and Halig, 2012. Hyperspectral Imaging and Spectral-Spatial Classification for Cancer Detection. Proceedings of *Biomedical Engineering and Informatics (BMEI) 5th International Conference*, Chongqing, China, pp.62-64.

[11] M. Fauvel, J. Benediktsson, J. Chanussot and J. Sveinsson, 2008. Spectral and Spatial Classification of Hyperspectral Data Using SVMs and Morphological Profiles. In *Geoscience and Remote Sensing, IEEE Transactions*, Vol. 46, Issue 11, pp 3804-3814.